Microwave Assisted Switching of Single Domain $Ni_{80}Fe_{20}$ Elements

Georg Woltersdorf and Christian H. Back

Universität Regensburg, Universitätsstraße 31, 93040 Regensburg, Germany

(Received 16 July 2007; published 30 November 2007; publisher error corrected 3 December 2007)

We study the switching behavior of thin single domain magnetic elements in the presence of microwave excitation. The application of a microwave field strongly reduces the coercivity of the elements. We show that this effect is most profound at the ferromagnetic resonance frequency of the elements. Observations using time-resolved magneto-optic Kerr microscopy in combination with pulsed microwave excitation further support that the microwave assisted switching process is indeed based on the coherent motion of the magnetization.

DOI: 10.1103/PhysRevLett.99.227207 PACS numbers: 75.60.Jk, 75.30.Ds, 75.75.+a, 78.47.+p

In magnetic recording the increasing data rates require fast magnetization reversal in small magnetic elements. Thin magnetic elements in the deep submicron range of sizes favor a single domain state and often show a switching behavior as expected by the Stoner-Wohlfarth theory. However, due to the absence of magnetization reversal processes based on domain wall motion or buckling, this implies that for coherent Stoner-Wohlfarth magnetic switching a field larger than the magnetic anisotropy field needs to be applied along the magnetic easy axis for a duration of several nanoseconds. This long wait time is required since applying a magnetic field opposing the magnetization does not exert a torque on the magnetization and only thermal fluctuation or a small initial misalignment of the magnetic field can cause large angle precession of the magnetization. Finally the magnetization precesses into the direction parallel to the applied field due to relaxation processes. This slow and—if based on thermal fluctuations—to a large extent unpredictable process can be avoided in two ways. (i) Precessional or ballistic switching; in this case the magnetic field is applied perpendicular to the magnetization and the torque term of the equation of motion is used [1–3] to drive the magnetization reversal. This type of switching, however, requires a careful timing of pulse length τ and magnetic field amplitude B since a deviation from the product of $\tau \cdot B$ can lead to multiple switching and a loss of control of the final state [4]. (ii) An alternative route is to use an rf field perpendicular to the magnetization in order to assist the magnetic switching. The feasibility of this method was shown in magnetic nanoparticles by superconducting quantum interference magnetometry [5] and recently by magnetic force microscopy [6]. In this Letter time-resolved Kerr microscopy is employed to show that this mechanism is also present in micrometer-sized thin film elements. The static magnetization is probed by a time-resolved method based on the magneto-optic Kerr effect.

For a single spin the magnetization dynamics can be described by the Landau-Lifshitz-Gilbert equation of motion [7]:

$$\frac{d\vec{M}}{dt} = -\gamma\mu_0[\vec{M} \times \vec{H}_{\text{eff}}] + \frac{\alpha}{M}\left[\vec{M} \times \frac{d\vec{M}}{dt}\right], \qquad (1)$$

where $\vec{M}$ is the magnetization vector, $\vec{H}_{\text{eff}}$ is the effective magnetic field, α is the damping parameter, and $\gamma = g\mu_B/\hbar$ is the absolute value of the gyromagnetic ratio. The first term on the right-hand side determines the resonance frequency and the second term represents damping and leads to relaxation. For the measurements, we use a time and spatially resolved ferromagnetic resonance (FMR) technique based on the time-resolved magneto-optical Kerr (TRMOKE) effect combined with continuous wave (cw) excitation [8]. The spatial resolution of our Kerr setup is roughly 300 nm. Details concerning this technique can be found in [9]. The magnetic sample is excited by means of a cw rf field which is phase-locked to the laser pulses. By measuring the TRMOKE signal as a function of the time delay between microwave signal and optical probe one obtains amplitude and phase of the magnetic precession.

The layer structure of the samples is prepared by sputter deposition in UHV of 5 nm Al/2 nm $Ni_{80}Fe_{20}$/200 nm Au/5 nm Ti onto GaAs. A coplanar waveguide with a signal linewidth of 10 μm is subsequently defined by optical lithography and dry etching. The magnetic elements are structured in a second e-beam lithography and dry etching step. Two different element sizes were investigated: 0.7×1.4 μm^2 hexagons and 1.5×3.0 μm^2 hexagons. The $Ni_{80}Fe_{20}$ structures have a 1:2 aspect ratio and a 45° taper. The thickness of the magnetic elements is only 2 nm to ensure that the single domain state is the magnetic ground state [10]. A schematic outline of the sample structure with the relative orientations of the dc and rf magnetic fields is shown in Fig. 1. In addition, an optical microscope image of a typical sample is shown in the upper inset of Fig. 2. An unpatterned region on top of the signal line (not shown) was used to characterize the 2 nm thick $Ni_{80}Fe_{20}$ film.

From the Kittel plot shown in Fig. 2, magnetic anisotropy, g factor, and effective magnetization are extracted:

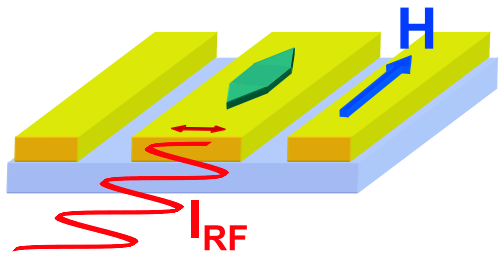

FIG. 1 (color online). Experimental configuration. A coplanar waveguide is used to excite the magnetic microstructures. The magnetic easy axis and the applied magnetic field are parallel to the coplanar waveguide.

$H_A = 0.1$ mT, $g = 2.2$, $\mu_0 M_{\text{eff}} = 0.93$ T. The damping parameter is determined from the frequency scan in a bias field of 5 mT and amounts to $\alpha = 0.0085$. The reduced M_{eff} is expected and a consequence of the perpendicular interface anisotropy present in such thin $Ni_{80}Fe_{20}$ films [11]. The zero-field resonance scan of the two hexagonal structures and the unpatterned films are compared in the lower inset of Fig. 2. The elongated hexagonal shape of the structures leads to a uniaxial shape anisotropy field along the long axis of the magnetic elements of about $\mu_0 H_A = 0.5$ mT for the larger and $\mu_0 H_A = 1.0$ mT for the smaller hexagon. This additional internal field in comparison with the extended film is evident in the 250 MHz and 700 MHz offsets of the zero-field resonance frequency, as can be seen in the lower inset of Fig. 2. As a consequence of the shape anisotropy, the two possible magnetic states of the elements (along the long axis of the elements pointing to the right or to the left) are thermally stable at room temperature. The energy barrier between the two states can be estimated from the uniaxial anisotropy field and leads—for example for the smaller element—to an energy barrier of 1 eV, which is far above $k_B T$ at 300 K. In the TRMOKE experiments indeed a stable single domain state is observed in zero field; see Fig. 3. This is important since we want to study the influence of a rf magnetic field on the switching behavior of magnetic elements immersed in an opposing magnetic field. The switching is studied by measuring hysteresis loops of an individual element. Figure 3 shows a typical example. The loops are acquired by using the off-resonance dynamic response to the synchronized microwave excitation measured by time-resolved Kerr microscopy. In the particular case shown in Fig. 3 we measure at a fixed frequency of 2 GHz. However, the resonance field of the element is at about 5 mT when it is excited at 2 GHz; see the inset of Fig. 2. This means that a field sweep from -1 mT to $+1$ mT is always far away from resonance and the induced precessional motion of the magnetization is small. Nevertheless, the technique applied here allows one to measure static hysteresis loops on individual magnetic

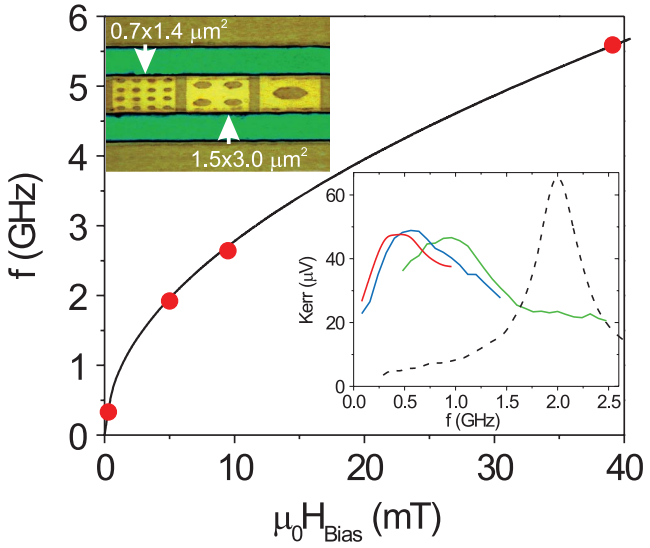

FIG. 2 (color). The main graph shows the Kittel plot for the $Ni_{80}Fe_{20}$ film. The resonance frequencies were determined by measuring the amplitude of the precession as a function of frequency at a low microwave power of 0 dBm. The inset on the top shows an optical microscope image of the microstructures. In the inset on the bottom resonance scans are shown. The red curve corresponds to the unpatterned $Ni_{80}Fe_{20}$ film. Blue and olive curves correspond to 1.5×3.0 μm^2 and 0.7×1.4 μm^2 hexagons, respectively. The microstructures have a built-in shape anisotropy of 0.5 mT and 1 mT leading to zero-field frequency offsets 250 and 700 MHz compared to the continuous film, respectively. The black dashed curve shows a resonance scan for the 1.5×3 μm^2 hexagon measured in a field of 5 mT.

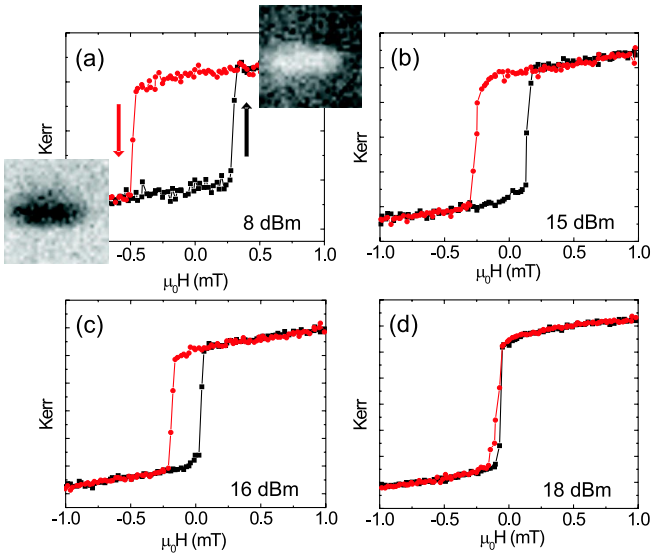

FIG. 3 (color online). Series of hysteresis loops measured for the 1.5×3 μm^2 hexagon as a function of microwave power at a fixed frequency of 2 GHz. The microwave frequency is 2 GHz with a power of (a) 8 dBm, (b) 15 dBm, (c) 16 dBm, and (d) 18 dBm. As the magnetization reverses, the sign of the magnetic response is inverted; see image scans in (a). The slight increase of the signal with increasing field is due to the fact that the amplitude of the magnetic precession increases with field since the resonance of the element at 2 GHz occurs at about 5 mT.

elements with an extremely high sensitivity: in the experiment the synchronized microwaves are chopped and lock-in detection is used. If the microwave field is applied in-plane and perpendicular to the magnetic easy axis of the elements, as illustrated in Fig. 1 the phase of the out-of-plane magnetic response to the microwaves changes by 180° (and hence the signal changes its sign) when the magnetization switches; see Fig. 3. Monitoring the polar Kerr signal as a function of the applied magnetic field therefore allows one to measure the magnetic hysteresis for individual elements as small as a few hundred nm. When hysteresis loops are measured as a function of microwave power at a fixed frequency one observes a gradually decreasing coercive field with increasing microwave power while the square shape of the hysteresis loop remains; Figs. 3 and 4 show the coercive field as a function of microwave power measured at a fixed frequency of 2 GHz. At a microwave power below 5 dBm the coercivity is independent of the power for both hexagonal element sizes. At a certain threshold power the coercivity is rapidly reduced to zero. The larger threshold power for the smaller hexagon can be expected due to its larger shape anisotropy. In a further experiment this collapse of the hysteresis was measured for applied microwave frequencies between 0.08 and 2.0 GHz. The result is shown in Fig. 5 in a 2D plot. One can clearly see that for a fixed microwave power the reduction of the coercivity is strongest at the 500 MHz resonance frequency of the $1.5 \times 3.0\ \mu m^2$ hexagon; cf. Fig. 2. This can be expected if the reduced coercivity is indeed caused by coherent motion of the magnetization dynamics, allowing the magnetization to spiral out of its local energy minimum when an opposing magnetic field is applied. Nembach *et al.* also recently observed a microwave induced reduction of the coercivity for much larger multidomain elliptical $Ni_{80}Fe_{20}$ elements ($160\ \mu m \times 80\ \mu m^2$) [12]. This reduction was explained by an enhanced domain wall nucleation in a microwave field [13] and preferential entropy-driven domain growth in a transverse microwave field [14]. In this Letter we show that for micron-sized single domain magnetic elements the microwave assisted switching is actually based on a coherent motion of the magnetization.

It is important to exclude the possibility that the reduction of the coercive fields is due to thermal heating effects. The large thickness of the Au waveguide underneath the 2 nm thick $Ni_{80}Fe_{20}$ film provides an efficient heat sink and the applied microwave power is small. The maximum applied power of 20 dBm corresponds to an in-plane rf-field amplitude of $h_{rf} \sim 4$ mT at $f = 2$ GHz for the 10 μm wide signal line. One can estimate the power absorbed at FMR using $P_{FMR} = \pi f \chi'' h_{rf}^2 A t_{FM}$ [15], where $\chi'' \sim 50$ is the imaginary part of the susceptibility at FMR and At_{FM} is the volume of the ferromagnetic sample. An upper limit for the expected heating ΔT at resonance can be estimated from steady state heating by the thermal conductivity of the substrate using the following relation: $\Delta T = \frac{tP_{FMR}}{\lambda}$, where $\lambda = 55$ W/mK for GaAs and $t = 200\ \mu$m is the thickness of the GaAs substrate. These pessimistic considerations only lead to a temperature increase of less than 0.2 K at FMR, in line with recent results reported in Ref. [16]. In addition to the magnetic dissipation there are also electrical losses in the 200 nm thick Au waveguide. Here the temperature increase can be estimated in the following way: in the frequency range of interest the waveguide has a transmission of more than $T = 90\%$. The 10 μm wide signal line section has a length of 1 mm. If one assumes that the losses are uniformly distributed along this length a dissipation of 10% of $P = 20$ dBm would lead to a temperature increase of only $\Delta T = \frac{t(1-T)P}{\lambda} \sim 4$ K. From these simple estimates one can see that heating

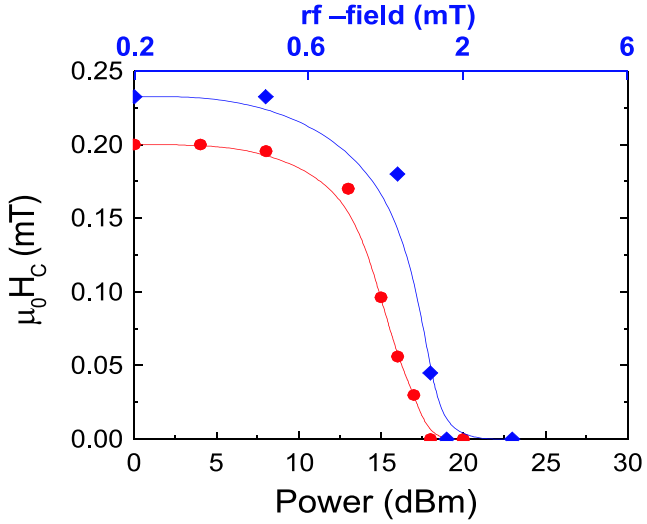

FIG. 4 (color online). Coercive field of the of the $0.7 \times 1.4\ \mu m^2$ (diamonds) and $1.5 \times 3.0\ \mu m^2$ (circles) hexagons as a function of microwave power at a frequency of 2 GHz.

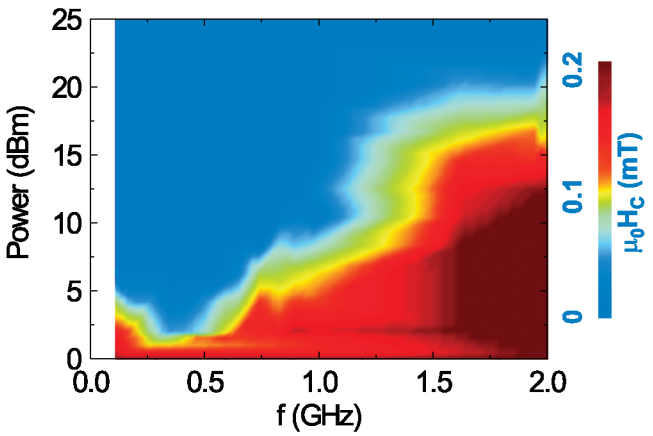

FIG. 5 (color). Coercive fields as a function of microwave power and frequency measured for the $1.5 \times 3.0\ \mu m^2$ hexagon. The zero-field resonance occurs at about 500 MHz (see lower inset in Fig. 2). The coercivity is color-coded and ranges between 0 and 0.4 mT. In addition to the power scale also a scale with the corresponding rf magnetic field is shown.

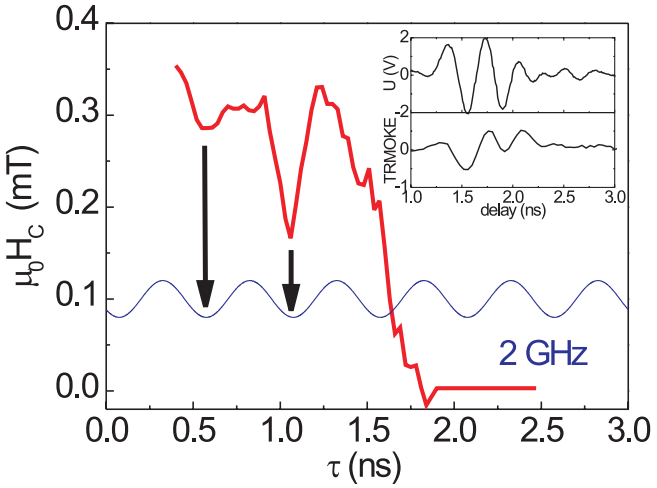

FIG. 6 (color online). Pulse length dependence of the coercive field measured for the 0.7×1.4 μm^2 hexagon. The pulse length is varied in 30 ps steps between 0.4 and 2.5 ns. The microwave carrier frequency is 2 GHz. The inset shows a 500 ps microwave burst acquired with a fast oscilloscope and the corresponding magnetic response.

cannot play a significant role in the reduction of the coercivity.

In order to further support the notion that the microwave assisted switching is related to a coherent motion of the magnetization, microwave bursts are used to study the switching behavior. Using a microwave mixer and a pulse generator short bursts with a carrier frequency of 2 GHz are produced from a 2 GHz cw signal. The rise and fall times of the pulses are about 200 ps and pulse lengths between 0.4 and 2.5 ns are studied. Typical microwave bursts generated by this method are shown in the inset of Fig. 6. In these measurements again the static magnetization is probed by the sign of the magnetic response to the microwave burst excitation. Figure 6 shows the coercive field as a function of the microwave pulse width at a constant microwave power of 18 dBm. The coercivity as a function of microwave burst duration is reduced in an oscillating manner. Dips of the coercive field are evidenced when the pulse period corresponds to a multiple of the period of the 2 GHz carrier frequency of the microwave burst (0.5 ns, 1.0 ns, and 1.5 ns). As the pulse length grows the precessional amplitude grows and it becomes more and more likely that the energy barrier may be overcome. This behavior is consistent with the picture that a coherent spin precession is the leading mechanism of the reduced coercivity. It is worthwhile to point out that although the duty cycle in the pulsed experiment is reduced by more than a factor of 6 compared to the experiments with cw excitation the peak amplitude required to cause a reduced coercivity remains nearly unchanged.

When the peak amplitude of the burst was reduced such that even for longer bursts (several ns) a finite coercivity can still be observed, a reduction of the coercivity is only observed for pulse lengths below approximately 2 ns. For longer pulses the coercivity is not reduced any further. This can be expected by considering the decay time of magnetic excitations. The decay time is determined from the damping parameter obtained from the frequency width of resonance scans at high fields (not shown): $\tau = 2/[\alpha\gamma\mu_0(M_{\mathrm{eff}} + 2H_{\mathrm{eff}})] = 1.4$ ns [17]. This implies that it is not possible to pump more energy into the magnetic system after 2 ns. The presence of this behavior also shows that thermal effects can be excluded since heating would simply lead to a continuous decrease of the coercivity as a function of pulse length.

In conclusion, it was shown that the coercive fields in micron-sized uniaxial magnetic elements can be significantly reduced in the presence of a rf magnetic field applied in-plane and perpendicular to the magnetization. This effect was shown to be a threshold effect. In addition, the reduction of the coercivity is strongest at the zero-field resonance frequency of the magnetic element itself. Measurements with short microwave pulses as a function of pulse length clearly show that the reduction of the coercive field is a consequence of coherent motion of the magnetization. The method which was used to measure the hysteresis loops by using the sign of the dynamic response as introduced in this Letter is new and provides an unprecedented signal-to-noise ratio allowing one to study magnetic switching behavior of individual submicron magnetic elements by magnetic Kerr effect microscopy.

Financial support from the DFG Priority Program No. 1133 and Sonderforschungsbereich No. 689 is gratefully acknowledged.

[1] C. H. Back *et al.*, Phys. Rev. Lett. **81**, 3251 (1998).
[2] T. Gerrits *et al.*, Nature (London) **418**, 509 (2002).
[3] W. Hiebert, L. Lagae, and J. de Boeck, Phys. Rev. B **68**, 020402 (2003).
[4] H. Schumacher *et al.*, Phys. Rev. Lett. **90**, 017204 (2003).
[5] C. Thirion, W. Wernsdorfer, and D. Mailly, Nature Mater. **2**, 524 (2003).
[6] Y. Nozaki *et al.*, Appl. Phys. Lett. **91**, 082510 (2007).
[7] L. D. Landau and E. Lifshitz, Phys. Z. Sowjetunion **8**, 153 (1935).
[8] S. Tamaru *et al.*, J. Appl. Phys. **91**, 8034 (2002).
[9] I. Neudecker *et al.*, J. Magn. Magn. Mater. **307**, 148 (2006).
[10] R. Cowburn *et al.*, Phys. Rev. Lett. **83**, 1042 (1999).
[11] J. O. Rantschler *et al.*, J. Appl. Phys. **97**, 10J113 (2005).
[12] H. T. Nembach *et al.*, Appl. Phys. Lett. **90**, 062503 (2007).
[13] E. Schloemann, IEEE Trans. Magn. **11**, 1051 (1975).
[14] A. Krasyuk *et al.*, Phys. Rev. Lett. **95**, 207201 (2005).
[15] A. G. Gurevitch, *Ferrites at RF Frequencies* (Springer, New York, 1960), Chap. 1, p. 1.
[16] R. Meckenstock *et al.*, J. Appl. Phys. **99**, 08C706 (2006).
[17] G. Woltersdorf *et al.*, Phys. Rev. Lett. **95**, 037401 (2005).